Magnetic Moment Measurements of 98Y Isomers Using the TDPAC Method at Lohengrin

D. Friant[1,2] J.M. Daugas[1] F. al-Khudair[3] A. Petrovici[4]
G. Georgiev[5] H. Haas[6] D. Kalaydjieva[7] U. Köster[1]
J. Röder[8] K. Stoychev[9]

[1]Institut Laue-Langevin, [2]CEA Saclay/BIOMAPS, [3]Uni. Basrah, [4]IFIN-HH, [5]CSNSM, [6]CERN, [7]Uni. Paris-Saclay, [8]LABOR AM ELM, [9]IJCLab

Fission 2026. March 9-13, 2026. Chamrousse

Background
Quantum Phase Transitions and Nuclear Deformation

- Phase Transitions capture qualitative changes.

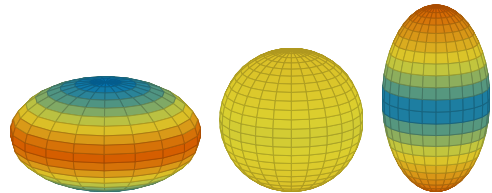

Figure 1: Schematics of the possible nuclear shape deformations.

[1] A. Frank, P. Van Isacker, & F. Iachello, 2006
[2] P. Cejnar, J. Jolie, & R. Casten, 2010

Background
Quantum Phase Transitions and Nuclear Deformation

- Phase Transitions capture qualitative changes.
- Quantum Phase Transitions have been found to come in two types[1]:

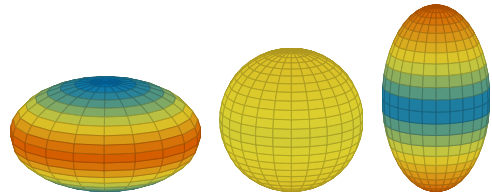

Figure 1: Schematics of the possible nuclear shape deformations.

[1] A. Frank, P. Van Isacker, & F. Iachello, 2006
[2] P. Cejnar, J. Jolie, & R. Casten, 2010

Background
Quantum Phase Transitions and Nuclear Deformation

- Phase Transitions capture qualitative changes.
- Quantum Phase Transitions have been found to come in two types[1]:
  1. $\hat{H} = (1 - \xi)\,\hat{H}_1 + \xi \hat{H}_2$

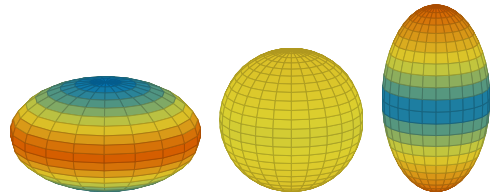

Figure 1: Schematics of the possible nuclear shape deformations.

[1] A. Frank, P. Van Isacker, & F. Iachello, 2006
[2] P. Cejnar, J. Jolie, & R. Casten, 2010

Background
Quantum Phase Transitions and Nuclear Deformation

- Phase Transitions capture qualitative changes.
- Quantum Phase Transitions have been found to come in two types[1]:
  1. $\hat{H} = (1-\xi)\,\hat{H}_1 + \xi \hat{H}_2$
  2. $\hat{H} = \begin{bmatrix} (1-\xi)\,\hat{H}_1 & \hat{W} \\ \hat{W} & \xi \hat{H}_2 \end{bmatrix}$

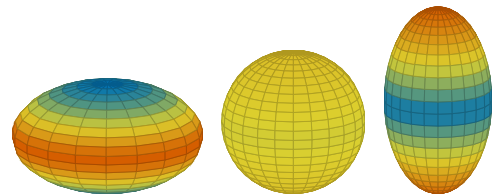

Figure 1: Schematics of the possible nuclear shape deformations.

[1] A. Frank, P. Van Isacker, & F. Iachello, 2006
[2] P. Cejnar, J. Jolie, & R. Casten, 2010

Background
Quantum Phase Transitions and Nuclear Deformation

- Phase Transitions capture qualitative changes.
- Quantum Phase Transitions have been found to come in two types[1]:
  1. $\hat{H} = (1-\xi)\,\hat{H}_1 + \xi \hat{H}_2$
  2. $\hat{H} = \begin{bmatrix} (1-\xi)\,\hat{H}_1 & \hat{W} \\ \hat{W} & \xi \hat{H}_2 \end{bmatrix}$
- QPTs in shape deformation of nuclei[2] provide a rich testing ground for nuclear models.

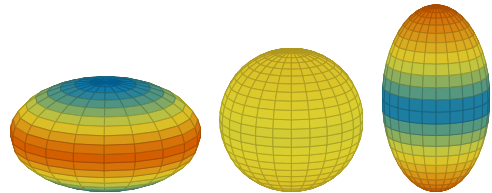

Figure 1: Schematics of the possible nuclear shape deformations.

[1] A. Frank, P. Van Isacker, & F. Iachello, 2006
[2] P. Cejnar, J. Jolie, & R. Casten, 2010

Background
Quantum Phase Transition in the $A \approx 100$ Region

- The neutron rich $A \approx 100$ region provides just such a testing ground.

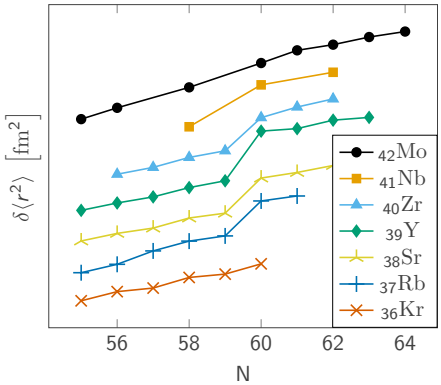

Figure 2: The mean-square charge radius for isotopes in the $A \approx 100$ region[3] with an arbitrary vertical offset per series.

[3] I. Angeli & IAEA, 1999

Background
Quantum Phase Transition in the $A \approx 100$ Region

- The neutron rich $A \approx 100$ region provides just such a testing ground.
- Only two added neutrons result in a substantial change from approx. spherical to prolate.

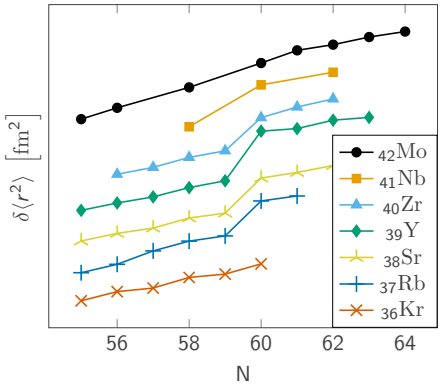

Figure 2: The mean-square charge radius for isotopes in the $A \approx 100$ region[3] with an arbitrary vertical offset per series.

[3] I. Angeli & IAEA, 1999

Background
Quantum Phase Transition in the $A \approx 100$ Region

- The neutron rich $A \approx 100$ region provides just such a testing ground.
- Only two added neutrons result in a substantial change from approx. spherical to prolate.
- This rapid change implies a strong reordering and distribution of individual energy levels and collective excitations.

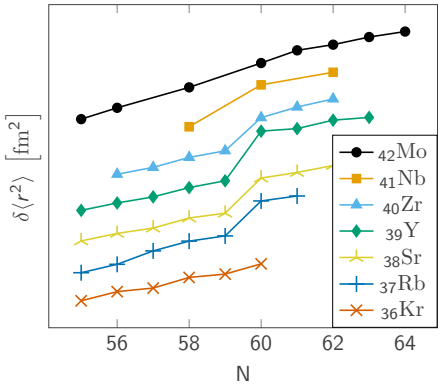

Figure 2: The mean-square charge radius for isotopes in the $A \approx 100$ region[3] with an arbitrary vertical offset per series.

[3] I. Angeli & IAEA, 1999

Background
Quantum Phase Transition in the $A \approx 100$ Region

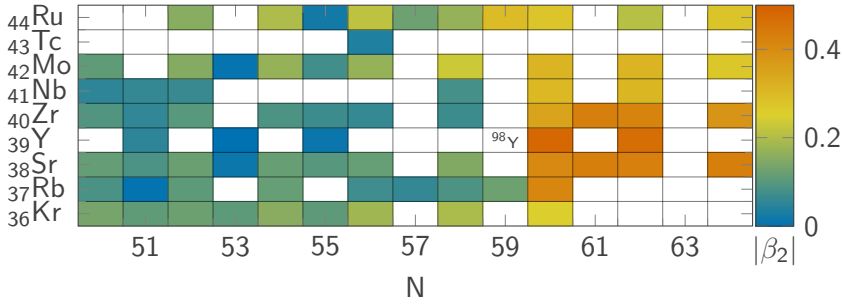

Figure 3: Ground-state quadrupole deformation parameter $|\beta_2|$ from nearly spherical (blue), to highly deformed (red).[4,5] Non-even-even values calculated from available spectroscopic quadrupole moment values.[6]

[4] ENSDF, 2026
[5] Albers et al. 2012
[6] Stone, 2021

Background
Shape Coexistence and Intertwined QPT

- Nuclear shape coexistence is defined as the occurrence of different nuclear shape deformations at similar energies within the same nucleus.[7]

[7] P. Garrett, M. Zielińska, & E. Clément, 2022
[8] W. Urban, M. Czerwiński, J. Kurpeta, et al. 2017
[9] N. Gavrielov, A. Leviatan, & F. Iachello, 2019

Background
Shape Coexistence and Intertwined QPT

- Nuclear shape coexistence is defined as the occurrence of different nuclear shape deformations at similar energies within the same nucleus.[7]
- Previous work has found substantial shape coexistence in ^{98}Y, providing good cause to measure its excited states.[8]

[7] P. Garrett, M. Zielińska, & E. Clément, 2022
[8] W. Urban, M. Czerwiński, J. Kurpeta, et al. 2017
[9] N. Gavrielov, A. Leviatan, & F. Iachello, 2019

Background
Shape Coexistence and Intertwined QPT

- Nuclear shape coexistence is defined as the occurrence of different nuclear shape deformations at similar energies within the same nucleus.[7]
- Previous work has found substantial shape coexistence in ^{98}Y, providing good cause to measure its excited states.[8]
- The closely related Zr isotopes have been modeled as IQPTs which allow for the mixing of type 1 and type 2 QPT.[9]

[7] P. Garrett, M. Zielińska, & E. Clément, 2022
[8] W. Urban, M. Czerwiński, J. Kurpeta, et al. 2017
[9] N. Gavrielov, A. Leviatan, & F. Iachello, 2019

Background
Shape Coexistence and Intertwined QPT

- Nuclear shape coexistence is defined as the occurrence of different nuclear shape deformations at similar energies within the same nucleus.[7]
- Previous work has found substantial shape coexistence in ^{98}Y, providing good cause to measure its excited states.[8]
- The closely related Zr isotopes have been modeled as IQPTs which allow for the mixing of type 1 and type 2 QPT.[9]
- In short, the neutron-rich $A \approx 100$ region is very rich (complex), and there is a great deal of work that remains to be done to both measure the EM moments and accurately model the isotopes here.

[7] P. Garrett, M. Zielińska, & E. Clément, 2022
[8] W. Urban, M. Czerwiński, J. Kurpeta, et al. 2017
[9] N. Gavrielov, A. Leviatan, & F. Iachello, 2019

Measurements

Overview

- Goal: measure the g-factors of the 375keV (4^-) and 171keV (2^-) states of ^{98}Y.

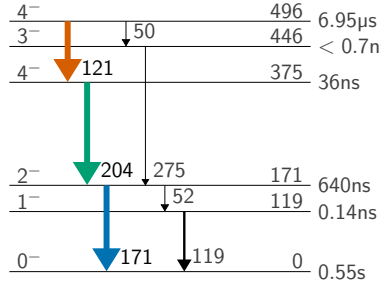

Figure 4: A partial level scheme of ^{98}Y showing the relevant de-excitation cascades.[8]

[8] ENSDF, March 2026.

Measurements

Overview

- Goal: measure the g-factors of the 375keV (4^-) and 171keV (2^-) states of ^{98}Y.
- Use the Lohengrin Mass Separator to isolate the excited isotopes.

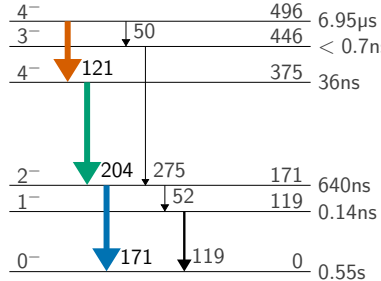

Figure 4: A partial level scheme of ^{98}Y showing the relevant de-excitation cascades.[8]

[8] ENSDF, March 2026.

Measurements

Overview

- Goal: measure the g-factors of the 375keV (4^-) and 171keV (2^-) states of ^{98}Y.
- Use the Lohengrin Mass Separator to isolate the excited isotopes.
- Use an external magnetic field to induce Larmor precession, and use the Time Differential Perturbed Angular Correlation (TDPAC) method to measure the frequency.

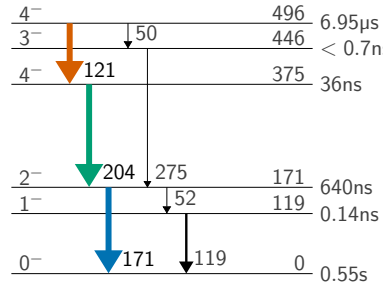

Figure 4: A partial level scheme of ^{98}Y showing the relevant de-excitation cascades.[8]

[8] ENSDF, March 2026.

Measurements

Overview

- Goal: measure the g-factors of the 375keV (4^-) and 171keV (2^-) states of ^{98}Y.
- Use the Lohengrin Mass Separator to isolate the excited isotopes.
- Use an external magnetic field to induce Larmor precession, and use the Time Differential Perturbed Angular Correlation (TDPAC) method to measure the frequency.
- Deduce the magnitude of the g-factor from the frequency and, if possible, the sign from the direction of the precession.

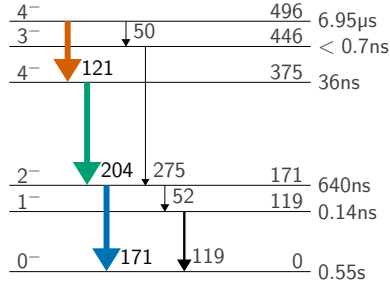

Figure 4: A partial level scheme of ^{98}Y showing the relevant de-excitation cascades.[8]

[8] ENSDF, March 2026.

Measurements
Lohengrin

- Lohengrin (PN1) uses the reactor at ILL to induce fission in a target channels the fragments out of the reactor.

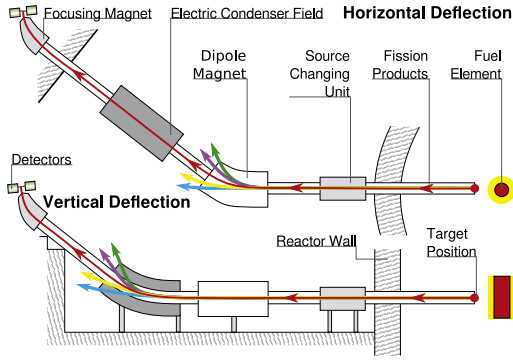

Figure 5: A schematic of the Lohengrin Mass Separator (PN1) at ILL.

Measurements
Lohengrin

- Lohengrin (PN1) uses the reactor at ILL to induce fission in a target channels the fragments out of the reactor.
- Isotope selection is done in two-stages: first a magnetic dipole then an electric condenser.

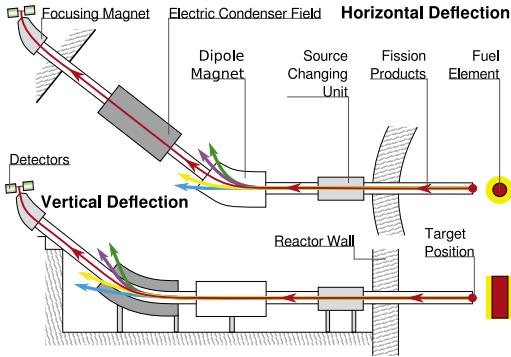

Figure 5: A schematic of the Lohengrin Mass Separator (PN1) at ILL.

Measurements
Lohengrin

- Lohengrin (PN1) uses the reactor at ILL to induce fission in a target channels the fragments out of the reactor.
- Isotope selection is done in two-stages: first a magnetic dipole then an electric condenser.
- The isotopes are deflected into modifiable experimental area and focused with a RED magnet.

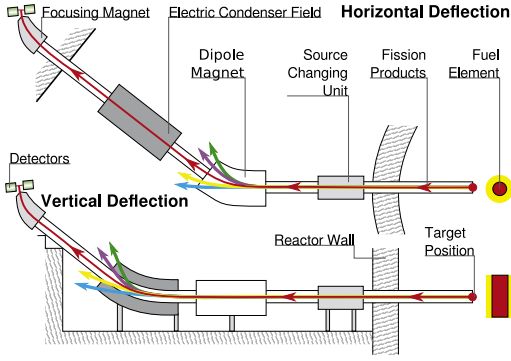

Figure 5: A schematic of the Lohengrin Mass Separator (PN1) at ILL.

Measurements
Experimental Setup and TDPAC

- The fission fragments are embedded into a foil at the focal plane of the beam.

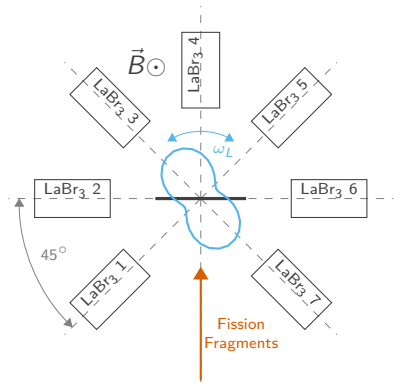

Figure 6: A schematic of the experimental apparatus used to perform the TDPAC measurements.

Measurements
Experimental Setup and TDPAC

- The fission fragments are embedded into a foil at the focal plane of the beam.
- The magnetic field induces precession, and the de-excitation γ are captured in an array of $LaBr_3$ scintillators attached to SiPM for conversion to electronic signal.

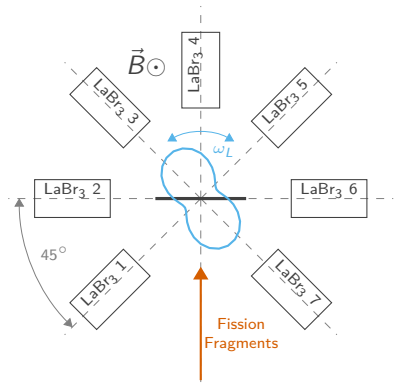

Figure 6: A schematic of the experimental apparatus used to perform the TDPAC measurements.

Measurements
Experimental Setup and TDPAC

- The fission fragments are embedded into a foil at the focal plane of the beam.
- The magnetic field induces precession, and the de-excitation γ are captured in an array of $LaBr_3$ scintillators attached to SiPM for conversion to electronic signal.
- Using one de-excitation as a trigger, we then measure other events in coincidence with it to identify angularly-perturbed cascades (TDPAC).

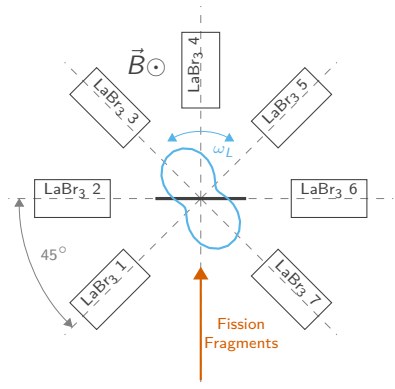

Figure 6: A schematic of the experimental apparatus used to perform the TDPAC measurements.

- Select the events of interest from those found in coincidence.

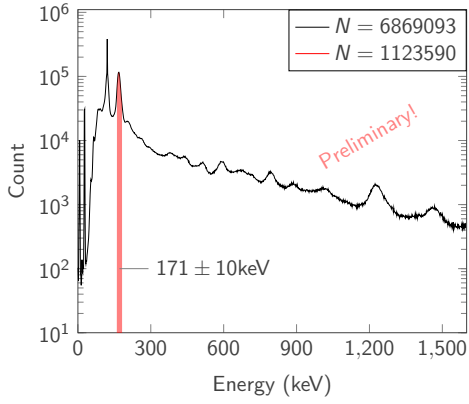

Figure 7: The energy distribution of all events found in coincidence with 204±10keV events.

- Select the events of interest from those found in coincidence.
- Check the quality of the selection via the half-life.

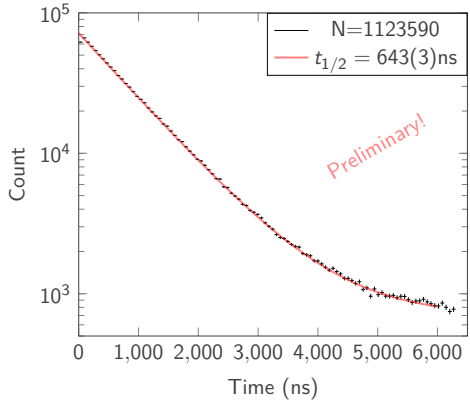

Figure 8: The measured and fit half-life of the 171keV state.

Measurements
Data Analysis

- Select the events of interest from those found in coincidence.
- Check the quality of the selection via the half-life.
- Compute the angular anisotropy and derive the precession frequency:

$$R(t) = \frac{\mathrm{I}(t,\theta) - \mathrm{I}(t,\pm\pi/2+\theta)}{\mathrm{I}(t,\theta) + \mathrm{I}(t,\pm\pi/2+\theta)}$$

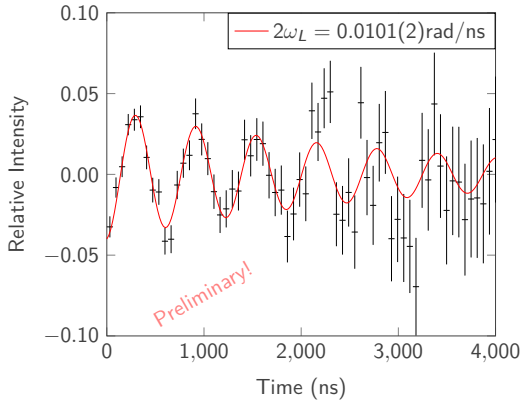

Figure 9: The relative intensity function $R(t)$ using all pairs of detectors at $\pm 90°$.

Measurements
Data Analysis

- Select the events of interest from those found in coincidence.
- Check the quality of the selection via the half-life.
- Compute the angular anisotropy and derive the precession frequency:
$$R(t) = \frac{\mathrm{I}(t,\theta) - \mathrm{I}(t,\pm\pi/2+\theta)}{\mathrm{I}(t,\theta) + \mathrm{I}(t,\pm\pi/2+\theta)}$$
- Determine the direction of the precession with respect to the magnetic field.

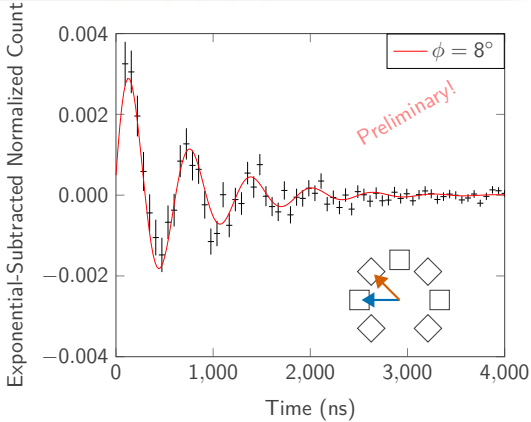

Figure 10: Measuring the direction of the Larmor precession using detectors separated by 45°.

Measurements
Data Analysis

- Select the events of interest from those found in coincidence.
- Check the quality of the selection via the half-life.
- Compute the angular anisotropy and derive the precession frequency:
$$R(t) = \frac{\mathrm{I}(t,\theta) - \mathrm{I}(t,\pm\pi/2+\theta)}{\mathrm{I}(t,\theta) + \mathrm{I}(t,\pm\pi/2+\theta)}$$
- Determine the direction of the precession with respect to the magnetic field.

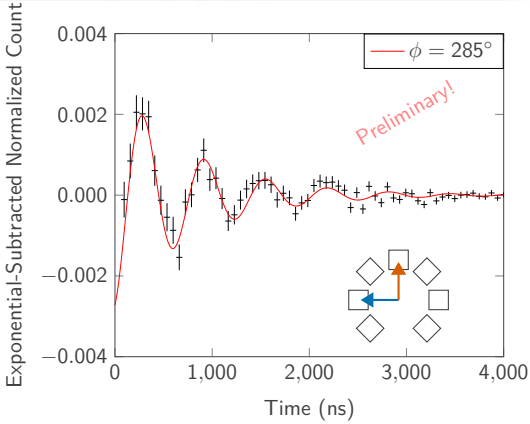

Figure 10: Measuring the direction of the Larmor precession using detectors separated by 90°.

Measurements
Data Analysis

- Select the events of interest from those found in coincidence.
- Check the quality of the selection via the half-life.
- Compute the angular anisotropy and derive the precession frequency:
$$R(t) = \frac{\mathrm{I}(t,\theta) - \mathrm{I}(t,\pm\pi/2+\theta)}{\mathrm{I}(t,\theta) + \mathrm{I}(t,\pm\pi/2+\theta)}$$
- Determine the direction of the precession with respect to the magnetic field.

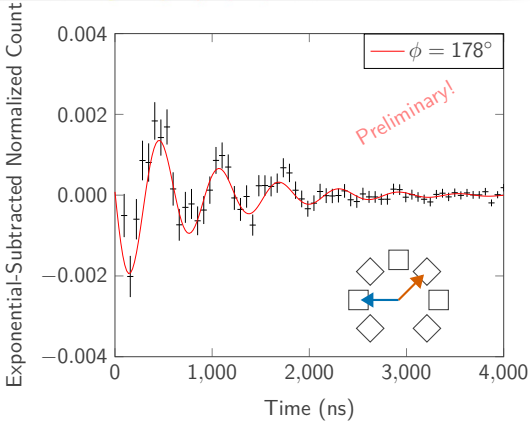

Figure 10: Measuring the direction of the Larmor precession using detectors separated by 135°.

Measurements
Data Analysis

- Select the events of interest from those found in coincidence.
- Check the quality of the selection via the half-life.
- Compute the angular anisotropy and derive the precession frequency:
$$R(t) = \frac{\mathrm{I}(t,\theta) - \mathrm{I}(t,\pm\pi/2+\theta)}{\mathrm{I}(t,\theta) + \mathrm{I}(t,\pm\pi/2+\theta)}$$
- Determine the direction of the precession with respect to the magnetic field.

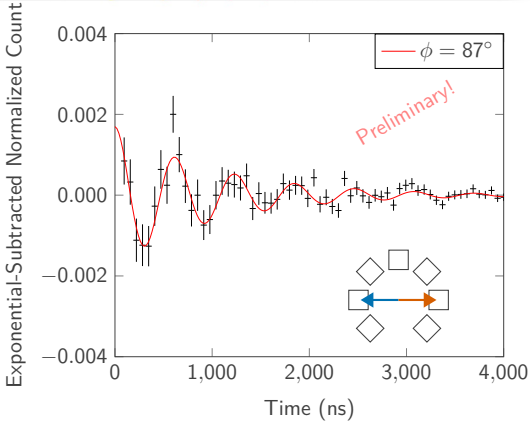

Figure 10: Measuring the direction of the Larmor precession using detectors separated by 180°.

Theory Comparison
Level Schemes

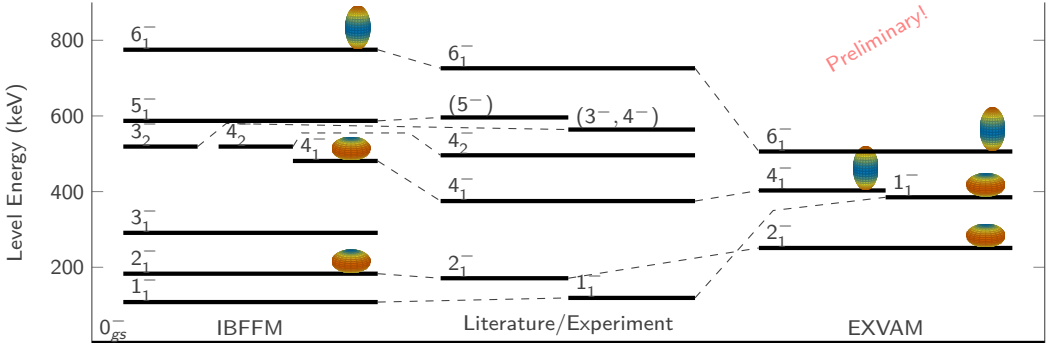

Figure 11: A three way comparison of the partial level scheme between experimental measurements, the Interacting Boson Fermion Fermion Model, and the *complex* EXcited VAMpir model.

Theory Comparison
Partial Occupancies

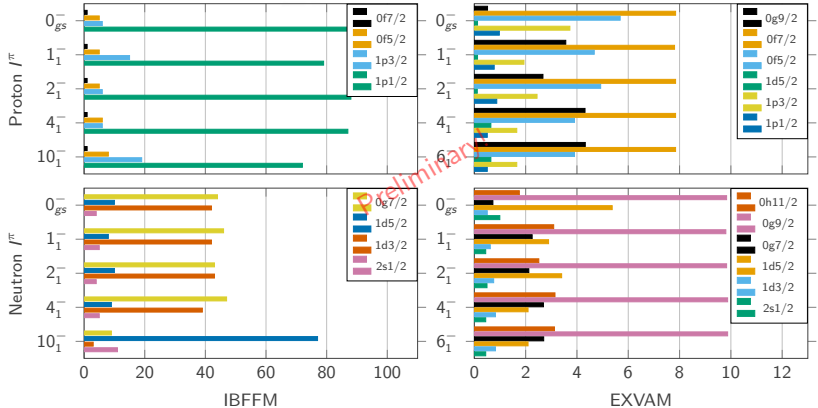

Figure 12: The partial wave function occupations for the unpaired neutron and proton in ^{98}Y for both the IBFFM and EXVAM models.

Preliminary Results and Final Remarks

State	g-factor			Q (e·fm^2)		B(E2: $I^\pi \rightarrow (I-2)^\pi$)		
(keV (I^π))	EXP	IBFFM	EXVAM	IBFFM	EXVAM	EXP	IBFFM	EXVAM
171 (2^-)	+0.277(10)	0.219	0.38	-67.2	49.0	3.76(24)	3.729	3.13
375 (4^-)	+0.1600(45)	0.136	0.21	-29.3	-94.6	41.9(80)	5.491	8.54

- The comparison of theory and experiment is quite good for the 171keV state.

Preliminary Results and Final Remarks

State (keV (I^π))	g-factor			Q (e·fm^2)		B(E2: $I^\pi \rightarrow (I-2)^\pi$)		
	EXP	IBFFM	EXVAM	IBFFM	EXVAM	EXP	IBFFM	EXVAM
171 (2^-)	+0.277(10)	0.219	0.38	-67.2	49.0	3.76(24)	3.729	3.13
375 (4^-)	+0.1600(45)	0.136	0.21	-29.3	-94.6	41.9(80)	5.491	8.54

- The comparison of theory and experiment is quite good for the 171keV state.
- The 375keV state is slightly less successful, but still decent.

Preliminary Results and Final Remarks

State	g-factor			Q (e·fm^2)		B(E2: $I^\pi \rightarrow (I-2)^\pi$)		
(keV (I^π))	EXP	IBFFM	EXVAM	IBFFM	EXVAM	EXP	IBFFM	EXVAM
171 (2^-)	+0.277(10)	0.219	0.38	-67.2	49.0	3.76(24)	3.729	3.13
375 (4^-)	+0.1600(45)	0.136	0.21	-29.3	-94.6	41.9(80)	5.491	8.54

- The comparison of theory and experiment is quite good for the 171keV state.
- The 375keV state is slightly less successful, but still decent.
- Overall, this is all novel work on both sides.

Preliminary Results and Final Remarks

State (keV (I^π))	g-factor			Q (e·fm^2)		B(E2: $I^\pi \rightarrow (I-2)^\pi$)		
	EXP	IBFFM	EXVAM	IBFFM	EXVAM	EXP	IBFFM	EXVAM
171 (2^-)	+0.277(10)	0.219	0.38	-67.2	49.0	3.76(24)	3.729	3.13
375 (4^-)	+0.1600(45)	0.136	0.21	-29.3	-94.6	41.9(80)	5.491	8.54

- The comparison of theory and experiment is quite good for the 171keV state.
- The 375keV state is slightly less successful, but still decent.
- Overall, this is all novel work on both sides.
- Future plans:

Preliminary Results and Final Remarks

State (keV (I^π))	g-factor			Q (e·fm^2)		B(E2: $I^\pi \rightarrow (I-2)^\pi$)		
	EXP	IBFFM	EXVAM	IBFFM	EXVAM	EXP	IBFFM	EXVAM
171 (2^-)	+0.277(10)	0.219	0.38	-67.2	49.0	3.76(24)	3.729	3.13
375 (4^-)	+0.1600(45)	0.136	0.21	-29.3	-94.6	41.9(80)	5.491	8.54

- The comparison of theory and experiment is quite good for the 171keV state.
- The 375keV state is slightly less successful, but still decent.
- Overall, this is all novel work on both sides.
- Future plans:
  - Finish the analysis of the quadrupole moment data.

Preliminary Results and Final Remarks

State (keV (I^π))	g-factor			Q (e·fm^2)		B(E2: $I^\pi \rightarrow (I-2)^\pi$)		
	EXP	IBFFM	EXVAM	IBFFM	EXVAM	EXP	IBFFM	EXVAM
171 (2^-)	+0.277(10)	0.219	0.38	-67.2	49.0	3.76(24)	3.729	3.13
375 (4^-)	+0.1600(45)	0.136	0.21	-29.3	-94.6	41.9(80)	5.491	8.54

- The comparison of theory and experiment is quite good for the 171keV state.
- The 375keV state is slightly less successful, but still decent.
- Overall, this is all novel work on both sides.
- Future plans:
  - Finish the analysis of the quadrupole moment data.
  - Explore the IPAC technique to push the bounds of possible measurements at Lohengrin down to the hundreds of ps.

Thanks

Dr. Falih Al-Khudair and Dr. Alexandrina Petrovici for allowing the use of yet-unpublished materials.

CEA Saclay/Biomaps for funding this work in part.


NEUTRONS
FOR SOCIETY
INSTITUT LAUE LANGEVIN